Multi-arm RNA junctions encoding molecular logic

unconstrained by input sequence for versatile cell-free

3 diagnostics

4 Duo Ma^{1,†}, Yuexin Li¹, Kaiyue Wu^{3,4}, Zhaoqing Yan^{3,4}, Anli A. Tang¹, Soma Chaudhary¹, Zachary M.

Ticktin¹, Jonathan Alcantar-Fenandez², Jose L. Moreno-Camacho², Abraham Campos-Romero²,

6 Alexander A. Green^{3,4,5}*

¹ Biodesign Center for Molecular Design and Biomimetics at the Biodesign Institute, Arizona

State University, Tempe, AZ 85287, USA

² Innovation and Research Department, Salud Digna, Culiacan, 80000, Sinaloa, Mexico

³ Department of Biomedical Engineering, Boston University, Boston, MA 02215, USA.

⁴ Molecular Biology, Cell Biology & Biochemistry Program, Graduate School of Arts and

Sciences, Boston University, Boston, MA 02215, USA

⁵ Biological Design Center, Boston University, Boston, MA 02215, USA

[†] Current address: Division of Biology and Biological Engineering, California Institute of

Technology, Pasadena, CA 91125, USA.

*Correspondence: aagreen@bu.edu

ABSTRACT

The central role of RNA in regulating gene expression and its predictable base pairing properties make it a powerful tool for implementing molecular circuits. However, applications of RNA-based molecular logic have been hampered by sequence constraints imposed on circuit input and output species that limit their potential applications. Here we show that extended single-stranded RNA structures consisting of multi-arm junctions can be engineered to encode and robustly execute molecular logic with substantially reduced sequence constraints. In these systems, multi-arm junctions self-assembled upstream of a regulated gene are engineered to sequentially unfold in a programmed manner in response to different RNA input species to conditionally activate translation. To implement this strategy, we develop loop-initiated RNA activators (LIRAs) that provide high-performance translational regulation while abolishing all input and output sequence constraints. Integrating LIRAs with multi-arm junctions, we execute three-input OR and AND logic expressions in *E. coli* cells with fully sequence-independent input RNAs. We further deploy the multi-arm junction RNAs for detecting pathogens in colorimetric logic-enabled paper-based diagnostic assays, exploiting two-input AND logic to accurately

identify SARS-CoV-2 from clinical saliva samples. Multi-arm junction RNAs and LIRAs are powerful tools for sequence-independent molecular sensing and logic with biotechnological and diagnostic applications.

INTRODUCTION

RNA adopts diverse secondary and tertiary structures that enable it to perform a variety of different roles in the cell, from regulating gene expression and catalyzing chemical reactions to sensing small molecules and scaffolding proteins¹⁻⁵. RNA molecules designed to fold into diverse secondary structures have been used to tightly regulate gene expression at the transcriptional and translational levels in response to trans-acting RNAs^{6,7}, small molecules⁸, proteins⁹, or specified logic expressions^{10,11}, and have been used in strand-displacement systems for computing and imaging applications^{12,13}. Moreover, they have found use in low-cost systems for detection of viruses¹⁴⁻¹⁶, mutations¹⁷, and for water testing^{18,19}. At the same time, the structural diversity of RNA has been harnessed in RNA nanotechnology to generate a variety of RNA-based nanostructures with complex geometries through self-assembly^{20,21,22}. These structures are assembled from molecular building blocks featuring hairpins, multi-arm junctions, and other structural elements programmed to fold into prescribed structures through combinations of dangling end, kissing loop, and crossover interactions²³⁻²⁷. Such assemblies have enabled the production of multivalent nanoparticles carrying siRNA payloads²⁸⁻³⁰ and have also been synthesized within living cells enabling enzyme localization^{31,32}. They provide a wealth of different RNA structures that can be harnessed for programming cellular function.

Taking concepts from RNA nanotechnology and RNA-based regulation of gene expression^{33,34}, recent years have seen the development of self-assembly-driven molecular computing systems that operate in living cells and exploit the combined interactions of multiple carefully designed synthetic RNAs^{11,35-37}. Such ribocomputing devices act by modulating gene expression in response to specified combinations of input RNAs and take advantage of the predictability of RNA-RNA interactions to enable effective computer-based design. These systems have been used to carry out combinations of AND, OR, NAND, and NOR logic with up to a dozen inputs and have operated using complexes formed from as many as five distinct RNAs in living cells^{11,36}. The ribocomputing devices developed thus far however have had several significant limitations that constrain the range of input RNAs that they can monitor and the range of output proteins that they can produce. These systems have relied on hybridization between multiple input RNAs for implementing AND logic, limiting their use against natural transcripts that lack the necessary complementarity between sequences or requiring adapter

strands that reduce system output (Supplementary Fig. 1a). Moreover, encoding OR logic elements within RNA regions that are translated has required long open reading frames with high secondary structure placed immediately upstream of the output gene sequence (Supplementary Fig. 1b). These regions can impede ribosome processivity, causing wide variations in the expression levels of output gene depending on the input RNA¹¹, and lead to extended N-terminal peptide extensions with unpredictable effects on output protein folding (Supplementary Fig. 1b-c). Addressing these limitations requires alternative means of initiating RNA-RNA interactions to reduce sequence constraints and improved strategies for encoding molecular logic that minimize their impact on output gene sequence.

Herein we describe a new strategy for implementing molecular logic that exploits multi-arm junction RNA structures to regulate gene expression while eliminating input RNA sequence constraints and reducing sequence interference with the output gene for OR logic. These ribocomputing systems make use of loop-initiated RNA activator (LIRA) motifs that bind to input RNAs through extended loop domains and expose downstream functional domains for subsequent reactions. We show that LIRAs can be used as riboregulators to activate gene expression with high dynamic range and orthogonality in E. coli cells without imposing any sequence constraints on input RNAs and the output gene. Using these validated motifs, we generate logic gate RNAs that encode multi-input molecular logic by folding up single strands of RNA into multi-arm junctions actuated by independent LIRA modules (Fig. 1). The resulting gate RNA structures unfold in a prescribed manner as they interact with cognate input RNAs to activate gene expression when AND and OR logic expressions are satisfied. We use the multi-arm junctions to implement three-input AND and OR operations in E. coli using completely sequence-independent input RNAs. Porting these systems to paper-based cell-free transcription-translation reactions, we find that LIRAs can be designed to detect viral RNA sequences and coupled with isothermal amplification reactions to detect the dengue virus, norovirus, and yellow fever virus. Finally, we harness the capacity of multi-arm RNA junctions to detect sequence-independent inputs to implement paper-based molecular logic assays that use OR logic to tolerate sequence differences between HIV subtypes and AND logic to accurately identify SARS-CoV-2 in clinical saliva samples by targeting at two regions of the virus at the same time.

96 **RESULTS**

65

66 67

68

69

70

71

72

73

74

75

76

77

78

79

80

81

82

83

84

85

86

87

88

89

90

91

92

93

94

95

97

Multi-arm junctions for controlling gene expression

Our general strategy for regulating gene expression using multi-arm junctions is illustrated in Fig. 1. A multi-arm structure is placed at the 5' end of an mRNA and is followed by the coding sequence of the regulated gene. This configuration establishes strong secondary structures in the mRNA that conceal the ribosome binding site (RBS) and start codon necessary to initiate translation. As a result, translation is repressed unless complementary input RNAs bind and unwind the structure. The stem-loop arms of the structure act as sensors that provide binding sites for each of the input RNAs. The form of molecular logic evaluated by the multi-arm assembly is programmed by controlling the length and number of the sensor arms. OR logic is implemented using short sensor arms that remain "unlocked" and available for input RNA binding. Hybridization of either input RNA unwinds the cognate sensor arm through to the base stem to activate translation. To implement AND logic, all but one sensor arm is lengthened to establish a "locked" configuration that prevents binding by the corresponding input RNA. Binding of successive inputs unlocks additional sensor arms for input binding and ultimately allows the RNA strand to be fully unwound, activating translation of the downstream gene. Compared to other approaches for implementing logic-gated gene expression with RNAs, this strategy abolishes the need for any sequence correlations between input RNAs for AND operations. Moreover, it does not require extended N-terminal residues to be added to the output protein for OR operations, which can interfere with protein folding. Implementing this strategy, however, first required that we develop loop-based RNA-RNA interactions that functioned reliably in vivo to enable unwinding of the junction structure through binding to the sensor arms.

98

99

100

101

102

103

104

105

106

107

108

109

110

111

112

113

114

115

116

117

118

119

121

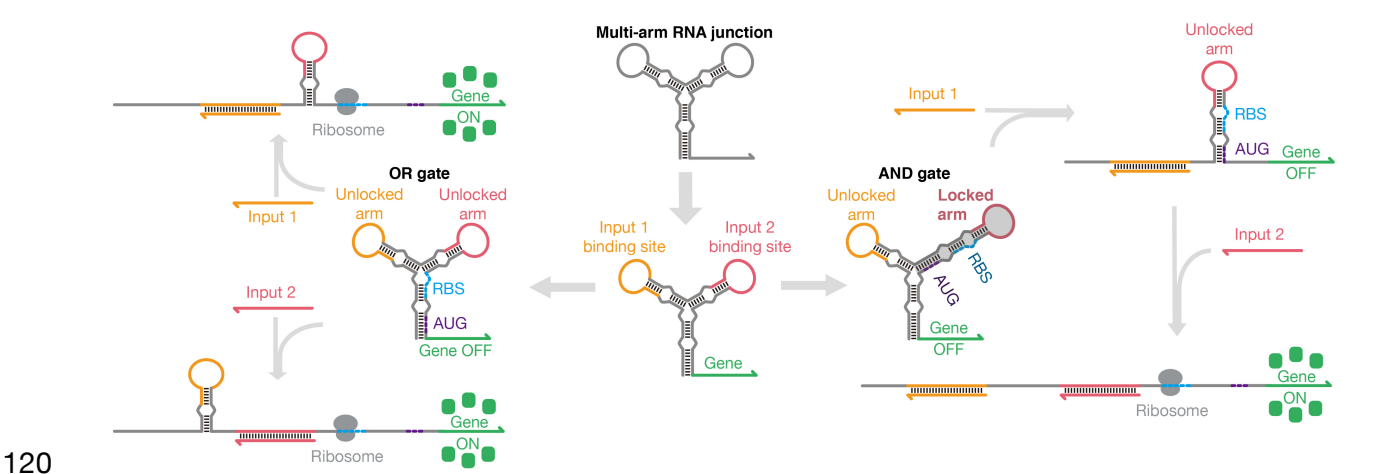


Fig. 1 | Design strategies for implementing sequence-independent RNA-based logic using multi-arm junctions. The three-arm junction in the schematic provides two sensing arms for

binding to complementary input RNAs and is positioned upstream of the regulated gene. Logic operations are encoded within the multi-arm junction structure by controlling the length and number of the stem-loop arms. Unlocked stem-loop arms enable direct binding of input RNAs and are used for OR logic. Locked arms are not available for binding to an input RNA until they are unlocked through binding of another input RNA species and are used for AND logic.

127128

129

130

131

132

133

134

135

136

137

138

139

140

141

142

143

144

145

146

147

148

149

150

151

152

153

154

155

123

124

125

126

Loop-initiated translational activation

We thus developed a set of riboregulators designed to be integrated into the stem-loop regions of multi-arm junctions. While many recent high-performance riboregulators, such as toehold switches⁷, have relied on single-stranded toehold domains to initiate reactions³⁸⁻⁴⁰, we hypothesized that long loop domains could be utilized to provide similar performance. Such long loops would provide a strong thermodynamic driving force to initiate RNA-RNA interactions and provide an input RNA binding site sufficiently labile and unconstrained to offer good reaction kinetics. Figure 2a shows the resulting loop-initiated RNA activators (LIRAs) that feature hairpins with extended loop domains regulating the expression of a downstream output gene. In the absence of the input RNA, translation by the LIRA is strongly repressed by sequestering both the RBS and the start codon of the output gene within the RNA duplex of the hairpin structure. A long loop domain a* of 21 nt is incorporated into the hairpin structure to promote the initial interaction between the LIRA and the activating RNA. After binding to the loop through the complementary a* sequence, the input RNA is designed to bind into the b* domain at the top of the hairpin stem, disrupting the existing base pairs and driving apart those located lower in the hairpin stem. Importantly, this effect enables the release of base pairs, in this case the RBS and start codon, that are completely unrelated to the sequence of the cognate input RNA. Thus, LIRAs can accommodate input RNAs without imposing any sequence constraints, and they can regulate a variety of different proteins without requiring modifications to the N-terminal sequence. In comparison, the design of toehold switch riboregulators causes three to four N-terminal residues in the output protein to be defined by the sequence of the input RNA (see Supplementary Fig. 2a), which prevents recognition of input RNAs that would generate stop codons upstream of the output gene7. To enable efficient expression and testing in vivo, four bulges were incorporated into the LIRA hairpin structure to reduce the likelihood of premature rho-independent transcriptional termination and to increase the thermodynamics driving the input-LIRA reaction. A 6-bp clamp domain was also added immediately after the start codon in the LIRA stem to reduce the likelihood of translational leakage (see Fig. 2a, Supplementary Fig.

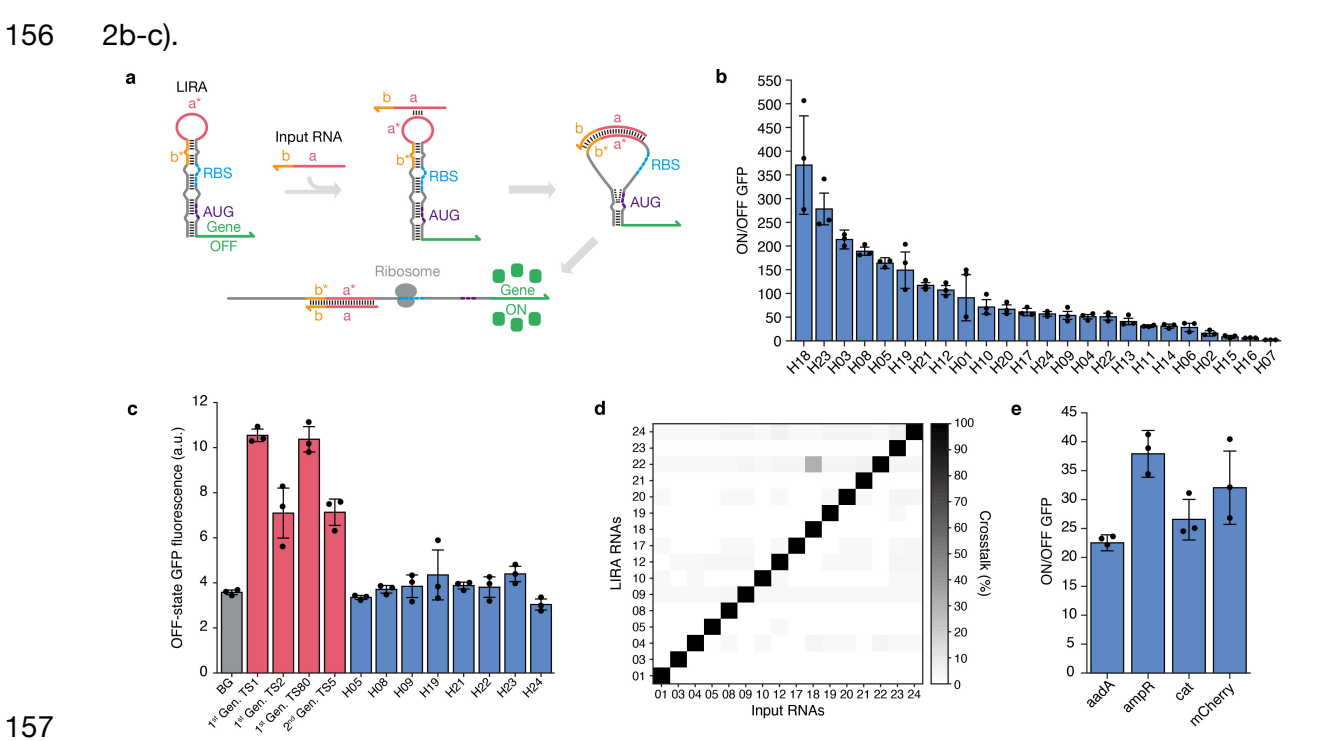


Fig. 2 | **Design and** *in vivo* validation of loop-initiated RNA activators (LIRAs). **a**, Schematic of the LIRA design and its interaction mechanism with the input RNA. Binding between the input RNA and the LIRA loop domain triggers release of the RBS and start codon (AUG) to activate translation. **b**, ON/OFF fluorescence ratios of a library of 24 different LIRAs. **c**, Leakage comparison of LIRAs and four toehold switches measuring GFP fluorescence in the absence of the input RNA. **d**, Crosstalk evaluation for 16 selected LIRA devices. **e**, Detection of full-length mRNAs using LIRAs. Measurements were taken 3 hours after induction with IPTG, n = 3 biological replicates, bars represent the geometric mean \pm SD.

A library of 24 different LIRA sequences were designed *de novo* using the NUPACK software package⁴¹ (see Methods) and plasmids were constructed to express the input and LIRA transcripts using T7 RNA polymerase in *E. coli* BL21 Star DE3 cells (see Supplementary Tables 1 and 2 for primer and LIRA sequence information). These experiments employed GFP as the reporter protein and measured fluorescence from the cells using flow cytometry. ON/OFF ratios for the LIRAs were determined by measuring the ON-state GFP expression in the presence of the cognate input and dividing it by the GFP expression measured in the OFF state where a non-cognate input was expressed in the cell (Fig. 2b, LIRA ON and OFF values are shown in Supplementary Fig. 3). We found that 16 out of 24 of the LIRAs provided ON/OFF ratios over 50-fold, with the highest one yielding an ON/OFF ratio of ~350-fold. Additional tests

using input RNAs complementary to different regions of the LIRA hairpin and different loop domain lengths revealed that the base LIRA design with a loop of 21 nt and a 31-nt input RNA provides the best overall performance (Supplementary Figs. 4 and 5, see Supplementary Tables 3 and 4 for sequence information).

177

178

179

180

181

182

183

184

185

186

187

188

189

190

191

192

193

194

195

196

197

198

199

200

201

202

203

204

205

206

207

208

209

We observed that multiple LIRAs provided very low translational leakage in the absence of the input RNA. Figure 2c shows the OFF-state GFP fluorescence of eight different LIRAs with ON/OFF ratios greater than 50 compared to the auto-fluorescence of cells lacking GFP and a set of previously reported toehold switch riboregulators with wide dynamic range⁷ (Supplementary Fig. 6a). We found that the toehold switches in the OFF-state yielded 2- to 3-fold higher fluorescence than the cells lacking GFP plasmids. In contrast, all eight of the LIRAs examined provided fluorescence leakage that was statistically indistinguishable from the background cellular fluorescence with p-values greater than 0.067 for all the LIRA devices in the plot compared to cell autofluorescence. Comparison of ON-state signals showed that three out of the four toehold switches provided higher signal output than the LIRAs (Supplementary Fig. 6b). To explain the very low OFF-state signals, we hypothesized that low-leakage LIRAs could be making use of a combined translational and transcriptional regulation mechanism to yield virtually undetectable leakage (Supplementary Fig. 6c), assisted by the strong secondary structure of the LIRA hairpin (see Supplementary Fig. 6d for comparison of minimum free energies for LIRA and toehold switch hairpins). To verify this hypothesis, we performed RT-qPCR experiments to measure the concentration of LIRA RNAs and cognate and non-cognate input RNAs expressed from cells in the ON and OFF states, respectively (Supplementary Fig. 7). We found that expression of the LIRA transcript with a non-cognate input was only 25% of that measured for the transcript with a cognate input, confirming that part of the LIRA regulation is due to transcriptional control. We also studied a set of four LIRA variants that contained different sequences in the stem below the start codon (see Supplementary Table 5 for sequence information), which in turn modify the N-terminal residues in the output protein. We found that these clamp sequence changes did not impact the OFF-state signal of the LIRAs (Supplementary Fig. 2c), but they did cause variations in ON-state expression levels ranging from 40% to 230% of the parent LIRA (Supplementary Fig. 2d). Despite these variations, all of the devices with clamp modifications displayed ON/OFF ratios of at least 50-fold (Supplementary Fig. 2e), indicating that changes in clamp sequence and the N-terminal residues are well tolerated by the riboregulators.

Foreshadowing their use in multi-arm junctions, we evaluated LIRA orthogonality by

measuring the crosstalk observed between the 16 devices providing the widest dynamic range. A 16x16 matrix of pairwise LIRA-input RNA interactions was measured by transforming cells with different combinations of plasmids. Figure 2d shows the measured crosstalk between the devices. Cognate interactions along the diagonal are normalized to 1 for the riboregulators in their ON states, while off-diagonal, non-cognate interactions reflect the percent activation with respect to the ON state. We found that crosstalk from the non-cognate inputs was very low, less than 4% in nearly all cases with a single strong off-target interaction observed between LIRA 22 and input 18 showing 5.6% crosstalk. Thus, the LIRAs provided a set of 15 orthogonal devices for regulation of gene expression *in vivo*.

Based on their low crosstalk and lack of sequence constraints, we also investigated if LIRAs could be designed to detect mRNAs within the cell. A set of LIRAs targeting regions of low secondary structure in the mRNAs for *mCherry* and the antibiotic resistance genes *aadA*, *ampR*, and *cat*, conferring resistance to spectinomycin, ampicillin, and chloramphenicol, respectively (see Supplementary Table 6 for sequence information). All LIRAs were based on a high-performance design identified during library screening and were generated simply by replacing the original target-binding site with the reverse complement of the mRNA target site. We found that all four mRNAs could be readily detected using the LIRAs and provided ON/OFF GFP levels ranging from 22- to 38-fold (Fig. 2e).

Multi-arm RNA junctions for in vivo molecular logic

Having developed a set of orthogonal LIRAs lacking sequence constraints, we next integrated them as sensing modules into the multi-arm RNA junction structures for computing intracellular OR and AND logic expressions. The sensing arms of the resulting logic gate RNA are each capped by different LIRA modules and designed to direct the unfolding of the structure as input RNAs bind to the gate RNA. Two-input OR logic devices were constructed upstream of a GFP reporter using a three-arm junction containing a pair of LIRA sensing arms (Fig. 3a). The base arm contains the RBS and start codon signals topped by the LIRA arms to provide binding sites A* and B* for interaction with the complementary input RNAs A and B. Binding of either input RNA disrupts the cognate stem-loop structure and further draws apart the base arm to reveal the RBS and start codon for translation initiation. To increase translational output for this input and reduce the likelihood of transcriptional regulation, we also incorporated a hairpin reconfiguration domain (indicated in dark blue in Fig. 3a) that generated an additional stem-loop upon binding of input A to the gate RNA. This newly formed stem disrupted the bottom gray

portion of the input B LIRA module, providing a single-stranded region upstream of the RBS and greater space to better accommodate the ribosomal footprint. During transcription, the hairpin domain can also help delay formation of the strong LIRA stem-loop structures to discourage transcriptional termination.

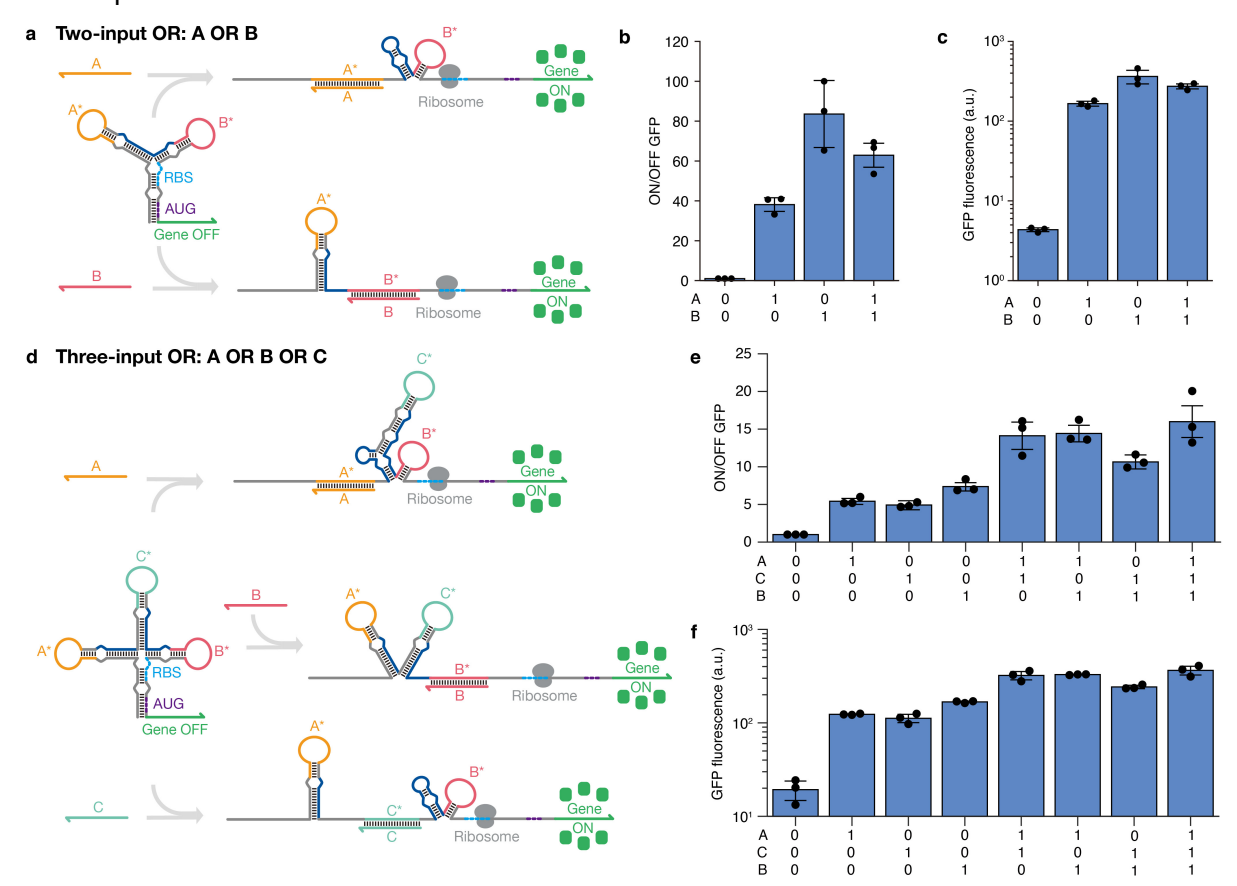


Fig. 3 | **Multi-arm RNA** junction molecular **OR** logic in *E. coli.* **a**, Schematic of a two-input OR logic gate RNA and its interaction mechanism with the input RNAs. **b**, ON/OFF fluorescence ratios of each input combination. **c**, GFP fluorescence of each input combination. **d**, Schematic of a three-input OR logic design and its interaction mechanism with the input RNAs. **e**, ON/OFF ratios of each input combination. **f**, GFP fluorescence of each input combination. All p values from two-tailed student's t-tests between each TRUE state and FALSE state are less than 0.05. Measurements were taken after 4 hours of IPTG induction, n = 3, bars represent the geometric mean \pm SD.

We tested the two-input OR device by transcribing the input and gate RNAs off separate high- and medium-copy plasmids, respectively, in *E. coli* (see Supplementary Table 7 for sequence information). Using flow cytometry, we found that GFP expression increased by 38- to

84-fold when any combination of the two input RNAs was expressed (Fig. 3b,c). We also constructed a three-input OR gate RNA using three orthogonal LIRA modules (Fig. 3d). This four-arm junction system contained a base arm with the RBS and start codon and inserted the LIRA stem loop for input C between modules for inputs A and B. Like the two-input device, the two left LIRA stem loops also contained hairpin reconfiguration domains to enable increased translation upon binding of inputs A and C. This circuit also performed as expected *in vivo* with low expression for the null-input logical FALSE case and 6- to 19-fold increases in expression when the input RNAs were expressed in any combination (Figure 3e,f).

Multi-arm junctions for AND logic employ sensor arms of different strengths to implement locked and unlocked LIRA sites (Fig. 4a). The gate RNA contains a base arm topped by a weak, unlocked sensor arm for LIRA module A* and a strong, locked sensor arm for LIRA module B*. The locked arm also conceals the RBS and start codon translation initiation signals within an RNA duplex. For the logical FALSE case when only input B is expressed, the locked stem-loop structure and the base stem are designed to be too thermodynamically stable to be disrupted by input RNA B, preventing system activation. However, if input A interacts with the gate RNA first, its binding energy is sufficiently strong to disrupt both the left stem loop and the base stem of the gate RNA. Unwinding the base stem in turn unlocks the LIRA B* module, making it sufficiently weak to interact with input B. Thus, when input B is also expressed, the B* module is completely disrupted and the RBS and start codon are exposed for translation of the GFP reporter gene. Unlike the LIRA OR gates, use of locked sensor arms for LIRA AND gates does add multiple N-terminal residues to the output protein (see Fig. 4a, Supplementary Fig. 1c).

We tested the two-input AND device in *E. coli* using different combinations of input RNAs (see Supplementary Table 7 for sequence information). We found that only strong GFP reporter expression was observed for the logical TRUE case with both inputs expressed. GFP expression increased by 79-fold for the TRUE case compared to the case with neither input transcribed (Fig. 4b,c). In addition, we found that translational leakage in the presence of input RNA B was low, 43-fold lower than the TRUE state, indicating that the extended stem-loop structure effectively blocked access of the transcript to the gate RNA. We also extended the AND ribocomputing strategy to three inputs using the four-arm junction structure shown in Fig. 4d. This device incorporated the binding site for input C to lock modules A* and B* and prevent them from interacting with their corresponding input RNAs without expression of input C. To increase translational output and encourage stem-loop disruption, hairpin reconfiguration

domains were added to the arms for inputs A and C. This device also functioned properly in *E. coli*, providing a 36-fold increase in GFP expression in the logical TRUE case with all three inputs expressed compared to the null-input case (Fig. 4e,f). Leakage in all logical FALSE conditions was low with the TRUE state providing at least 16-fold higher GFP output in all cases.

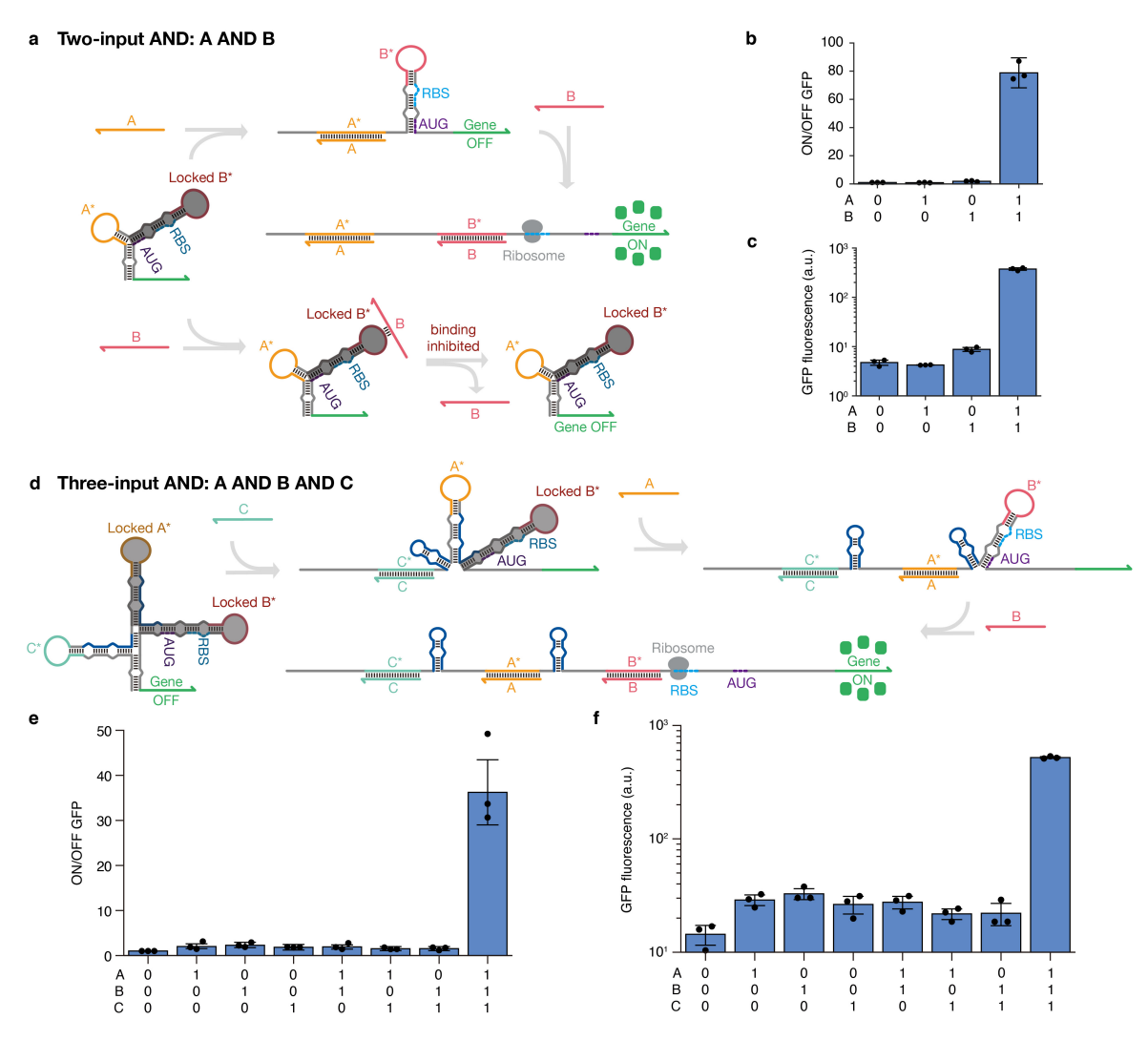


Fig. 4 | Multi-arm RNA junction molecular AND logic in *E. coli.* **a**, Schematic of the two-input AND logic design and its interaction mechanism with the input RNAs. **b**, ON/OFF fluorescence ratios for each input combination. **c**, GFP fluorescence for each input combination. **d**, Schematic of the three-input AND logic design and its interaction mechanism with the input RNAs. **e**, ON/OFF ratios for each input combination. **f**, GFP fluorescence for each input combination. All p values from two-tailed student's t-tests between each FALSE state and TRUE state are less than 0.05. Measurements were taken after 4 hours of IPTG induction, n = 3, bars

represent the geometric mean ± SD.

306 307

308

309

310

311312

313

314

315

316

317

318

319

320

321

322

323

324

325

326

327

328

329

330

331

332

333

334

335

336

337

338

Validation of LIRAs in paper-based diagnostics

The sensing and logic capabilities of LIRAs and multi-arm junction RNA structures also make them promising devices for use in paper-based cell-free systems, where they can be used as diagnostics without the need for expensive equipment and provide results that can be detected by the naked eye¹⁴⁻¹⁷. Since RNA-RNA interactions differ in cell-free reactions compared to the cytoplasmic environment, we first tested LIRAs by using them as riboregulators in paper-based reactions (see Supplementary Table 8 for sequence information). These reactions employed freeze-dried cell-free transcription-translation reactions along with LIRA plasmids, the lacZ ω subunit, and the lacZ colorimetric substrate CPRG (chlorophenol-red-β-d-galactopyranoside) deposited onto 2-mm diameter paper discs (Fig. 5a). At the time of use, the paper discs were rehydrated with solutions containing RNAs for detection by the embedded LIRA riboregulators. We first tested the paper-based reactions with LIRAs that showed wide dynamic range during in vivo experiments. However, in the cell-free reactions, they were unable to be turned on by their cognate input RNAs. To increase translational output and encourage stem-loop disruption, a hairpin reconfiguration domain was added to the 5' end of each LIRA sensor (Fig. 5b). Applying synthetic viral RNA targets to a final concentration of 5 µM, we found that the updated LIRA pathogen sensors provided strong increases in absorbance at 575 nm wavelength as the yellow-to-purple CPRG cleavage reaction was carried out by lacZ (Fig. 5c). Reactions with the pathogen RNAs turned to the expected pink or purple color as the reactions proceeded, while those without the pathogen RNAs remained yellow to yellow-pink in color depending on the sensor (Fig. 5c, bottom).

To enable detection of RNAs at the concentrations typically present in clinical samples, we used nucleic acid sequence-based amplification (NASBA) to amplify low-concentration pathogen RNAs prior to use in the paper-based assays. In NASBA, a combined reaction featuring reverse transcription, T7 RNA polymerase, RNase H, and DNA primers that incorporate the T7 promoter sequence are used to generate multiple RNA copies from a starting RNA template. Synthetic RNA targets from norovirus and yellow fever virus (YFV) were supplied to NASBA reactions at an initial concentration of 200 aM and amplified over 2 hours at 41°C. We found that both pathogen RNAs could be successfully detected in the colorimetric paper-based reactions following NASBA (Fig. 5d).

In addition, we applied the assay to a clinical serum samples positive and negative for

the dengue virus. The serum samples were first diluted by 10-fold into water and heated to 95°C for 2 minutes to release the viral genome from the capsid. The RNA was then amplified using NASBA and applied to the paper-based LIRA sensors. We found that LIRAs could unambiguously identify the clinical dengue sample through the resulting purple color. To determine the detection limit of the dengue assay, we carried out a series of NASBA/LIRA reactions with synthetic dengue target RNA concentrations ranging from 200 fM down to 0.2 aM. We found that the dengue transcript could be detected down to concentrations as low as 20 aM in the NASBA reaction, which corresponds to 12 RNA copies per µL of reaction (Fig. 5e).

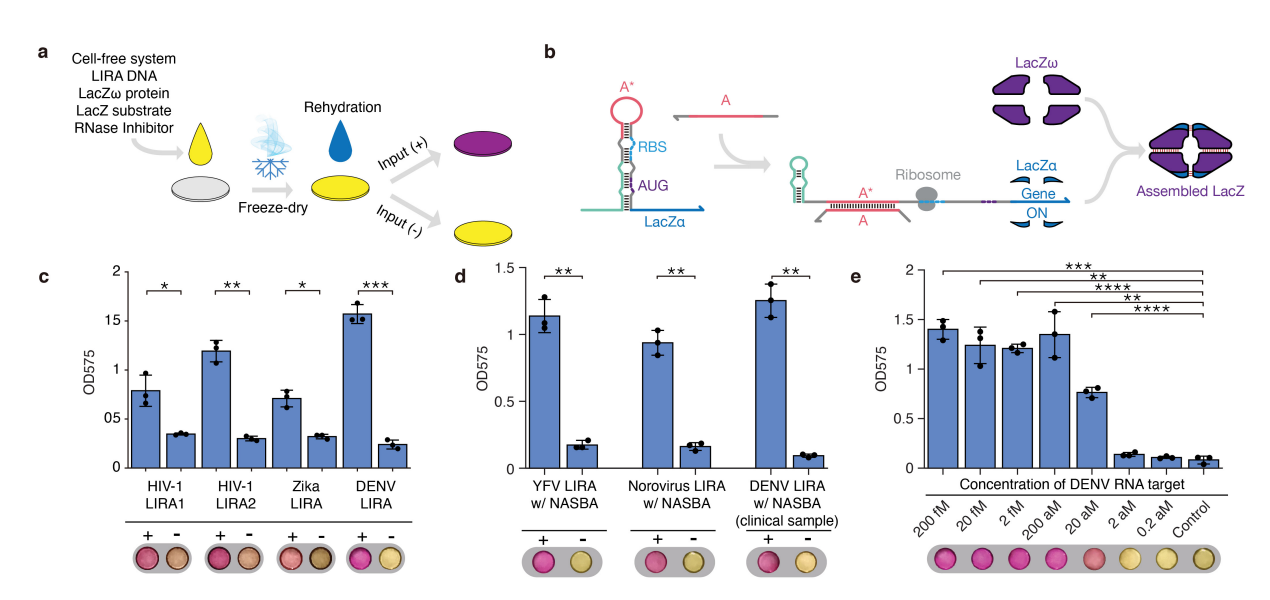


Fig. 5 | Pathogen-detecting LIRAs in paper-based cell-free assays. a, Schematic of paper-based diagnostic assays where cell-free transcription-translation reactions are freeze dried on paper disks to stabilize them at room temperature. Paper-based systems are reactivated by adding water with the RNA analyte of interest. b, LIRA design used for detection of viral RNAs in paper-based reactions. The optimized LIRA contains a 5' hairpin reconfiguration domain that forms after input RNA binding to assist with activating the LIRA and increasing output gene expression. c, Detection of synthetic RNA targets for HIV, the Zika virus, and the dengue virus (DENV) in 80-minute paper-based reactions. The purple color change of the disks is measured by the optical density at 575 nm (OD575) and indicates that the input RNA has been detected. d, Detection of viral RNA targets at initial concentrations of 200 aM after coupling with NASBA isothermal amplification and running cell-free reactions for 80 minutes for the yellow fever virus (YFV) and 90 minutes for norovirus. Clinical serum samples positive and negative for DENV were amplified by NASBA and detected after 90 minutes in paper-based

reactions containing a DENV-specific LIRA. **e**, Detection limit test of DENV at different starting concentrations of synthetic input RNAs demonstrating a limit of detection of 20 aM after 90-minute paper-based cell-free reactions. Two tailed student's t-test, *p<0.05, **p<0.01, ****p<0.001, ****p<0.0001, n = 3, bars represent the arithmetic mean \pm SD.

Paper-based diagnostic with embedded molecular logic

Diagnostic devices that combine visible readouts with the ability to perform information processing on biomolecular inputs have the potential to improve assay capabilities by expanding the number of pathogens a single test can detect, reducing false positives, and lowering assay complexity and cost. To demonstrate the potential of such logic-enabled paper-based diagnostic devices, we carried out proof-of-concept studies exploiting the logic capabilities of multi-arm junction molecular logic for HIV and SARS-CoV-2 detection. HIV continues to be a major global health threat with HIV-1 group M the predominant cause of infections worldwide^{42,43}. Within group M, there are nine different subtypes with genetic distances of 25% to 35% and prevalences that vary depending on the geographic region. HIV-1 subtype C causes >50% of infections worldwide and circulates mostly in India and regions of Africa, while HIV-1 subtype B predominates in Europe and the Americas⁴⁴. We thus aimed to develop a logic system capable of detecting both HIV-1 subtype B and C using a single OR operation, which could be deployed in an area such as Southern Brazil where both subtypes are common⁴⁵.

To implement the system, we first identified conserved regions in the genomes of HIV-1 subtypes B and C to use as circuit input RNAs. Complementary sequences for these inputs were then incorporated into a two-input OR three-arm junction gate RNA (Fig. 6a, see Supplementary Table 9 for sequence information). To ensure the system functioned properly in paper-based cell-free reactions, the binding site for the input RNAs was extended so that it included both the loop domain and the entire stem of the LIRA module. The gate RNA was transcribed in the cell-free reactions and supplied with the HIV-1 subtypes B and C input RNAs. For both inputs, output of the lacZ α subunit was produced as evidenced by increased production of the purple cleavage product in the paper-based reactions (Fig. 6b). Reactions lacking either input RNA remained yellow.

We next made use of AND logic operations to implement RNA devices for severe acute respiratory syndrome coronavirus 2 (SARS-CoV-2) detection. SARS-CoV-2 was first reported in 2019 in Wuhan, China, has now become a global pandemic with over 100 million reported

cases and over 3 million deaths worldwide according to the data from the Johns Hopkins Coronavirus Resource Center. SARS-CoV-2 can be transmissible even before any symptoms have developed^{46,47} and studies have shown that many patients who test positive for the virus do not show any symptoms⁴⁸. These factors have allowed the pandemic to take hold and emphasize the importance of developing diagnostic assays that can be widely deployed to detect SARS-CoV-2, even in carriers who do not have any signs of illness.

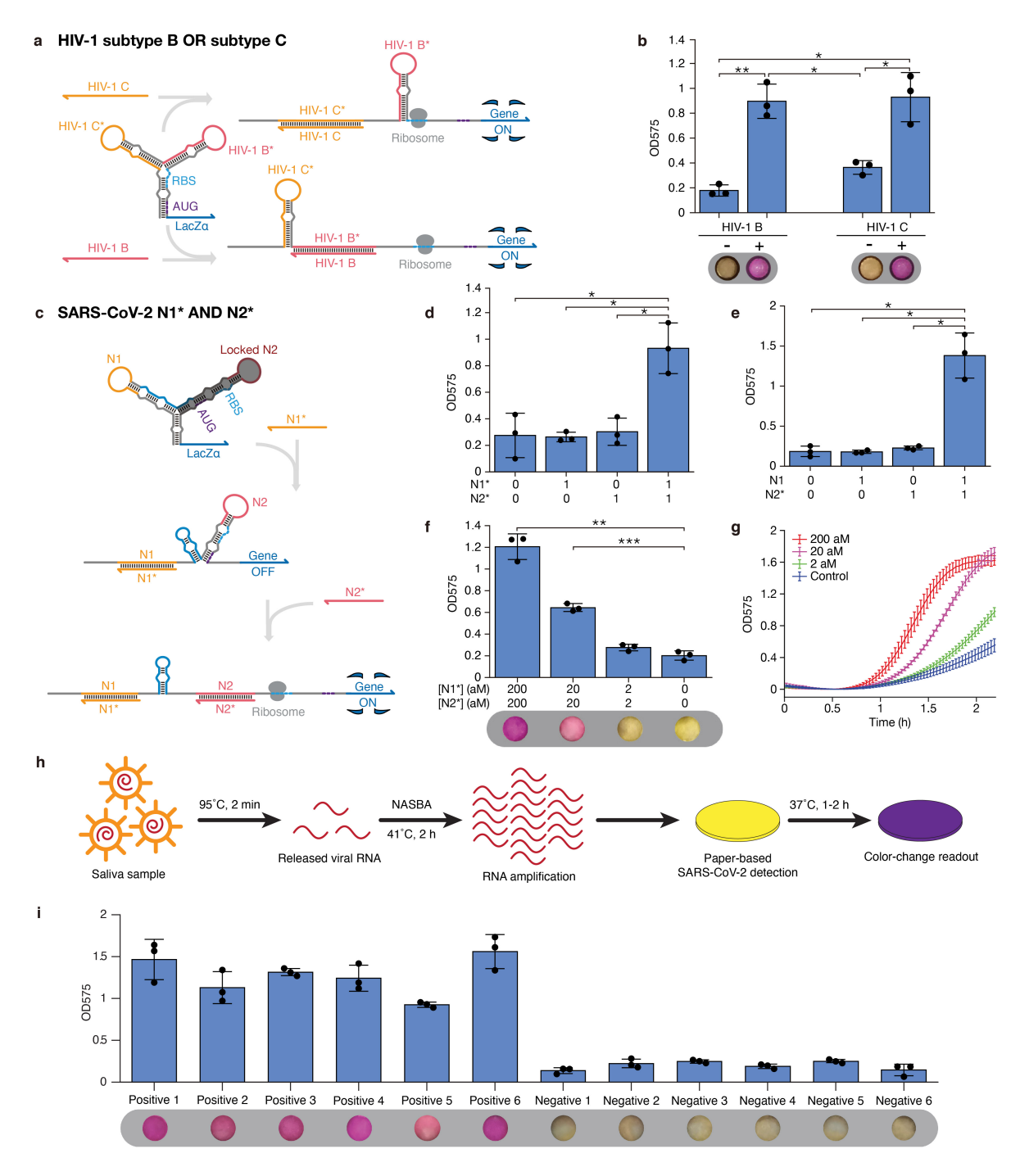


Fig. 6 | Logic-enabled paper-based tests using multi-arm junction gate RNAs for identification of HIV-1 group M subtypes and SARS-CoV-2. a, Schematic of the three-arm junction gate RNA used for simultaneous detection of B and C HIV-1 subtypes via two-input OR logic. b, Detection of HIV-1 B and HIV-1 C subtypes in paper-based reactions. Photographs are taken after 90 minutes of the cell-free reaction. c, Schematic of the three-arm junction gate RNA used for SARS-CoV-2 detection via two-input AND logic. d, OD575 for an AND gate RNA

N1*N2* detecting synthetic input fragments N1* and N2* from the SARS-CoV-2 genome. **e**, OD575 for an AND gate RNA N2*N1 detecting synthetic input fragments N2* and N1 from the SARS-CoV-2 genome. **f**, Validation of AND gate RNA N1*N2* with heat-inactivated SARS-CoV-2 virions amplified via isothermal NASBA reactions. Inactivated viruses were diluted with water. Photos were taken after 90-minute reactions. **g**, Time-course curves for the reactions tested in panel f. **h**, Schematic of the process for measuring clinical saliva samples starting from heat-driven RNA extraction through to the colorimetric paper-based cell-free assay. **i**, AND gate RNA N1*N2* tested with SARS-CoV-2 positive and negative saliva samples with NASBA products after 2-hour reactions, p values between each pair of positive and negative samples are all less than 0.05. Two tailed student's T test, *p<0.05, **p<0.01, ***p<0.001, ****p<0.0001. n = 3, curves represent arithmetic mean ± SD.

Following CDC recommendations⁴⁹, SARS-CoV-2 infections are often identified by amplification of two selected regions of the virus nucleocapsid (N) gene, 2019-nCoV_N1 and 2019-nCoV_N2. RT-qPCR is the most common method of detection of SARS-CoV-2 given its excellent specificity and sensitivity. However, it requires well-trained personnel and expensive equipment, which makes virus detection more challenging in rural areas with limited medical resources and requires additional time to ship samples to centralized facilities. Previous paper-based cell-free assays have been limited to detecting only a single pathogen target sequence at a time, and parallel assays that detect target RNAs in separate reactions can suffer as a result of differences in riboregulator activation speed and lead to increased assay cost.

To overcome these issues, we combined AND logic multi-arm junctions with isothermal amplification reactions to simultaneously detect two different SARS-CoV-2 N gene sequences using a single paper-based readout reaction. The resulting two-input AND gate RNAs contained a hairpin reconfiguration domain to encourage binding between the gate RNA and the input viral RNAs (Fig. 6c, see Supplementary Table 9 for sequence information). We first evaluated several devices using synthetic targets and identified two with the best performance. Gate RNA N1*N2* recognizes the antisense sequences in regions N1 and N2 of the SARS-CoV-2 N gene, with left and right sensor arms targeting N1* and N2*, respectively (Fig. 6d). Similarly, gate N2*N1 targets the antisense sequence of the N2 region with the left sensor arm and the sense sequence of the N1 region with the right sensor arm (Fig. 6e). Both devices show clear color changes in the presence of the two input RNAs, but did not activate when one or both inputs were absent, successfully carrying out AND logic (Fig. 6d,e).

We then designed specific NASBA primer pairs for each of the two devices to amplify the input RNAs from the SARS-CoV-2 genome. NASBA reactions were performed using heat-inactivated SARS-CoV-2 virus particles at a range of different concentrations. We found that gate N1*N2* performed better than gate N2*N1 and enabled detection of SARS-CoV-2 down to concentrations of 20 aM in the NASBA reactions when viewed by the naked eye (Fig. 6q), a concentration that is within the range necessary for detecting the virus in clinical samples⁵⁰. Using a plate reader, SARS-CoV-2 down to a concentration of 2 aM in the NASBA reaction could be distinguished. We then tested six positive saliva samples from SARS-CoV-2 patients together with six negative ones. Figure 6h illustrates the process from sample treatment to paper-based reactions. Diluted saliva samples were subjected to a brief 95°C heating step for 2 minutes to release the viral RNA and then added to NASBA reactions for amplification of each input RNA. The resulting amplicons were then applied to paper-based cell-free reactions for testing with the SARS-CoV-2 AND gate N1*N2* RNA. As shown in Figure 6i, the gate RNA successfully detected the six positive samples generating a clearly visible purple color while the six negative samples remained remain yellow color. A similar strategy was also applied to differentiate different influenza A subtypes and successfully distinguished H1N1. H5N1, and H1N2 from closely related virus subtypes (Supplementary Fig. 8, see Supplementary Table 10 for sequence information).

DISCUSSION

We have implemented a strategy for encoding molecular logic operations in multi-arm RNA junctions for regulation at the translational level. These systems make use of loop-initiated RNA-RNA interactions via LIRA modules to detect input RNAs and direct the programmed unfolding of the multi-arm RNA structures to report on computation results. We have found that LIRAs on their own can operate as riboregulators with wide dynamic range, good orthogonality, and low translational leakage using such loop interactions. Moreover, they completely decouple the sequence of their cognate input RNA from the sequence of the output module that they expose, which avoids some of the limitations of toehold-based riboregulators. By incorporating LIRA modules into the multi-arm junctions, we successfully implemented three-input OR and three-input AND operations in living *E. coli* cells. We also applied these systems in paper-based cell-free assays for detection of viruses, including the dengue virus and SARS-CoV-2 from clinical samples. Using multi-arm junctions in paper-based reactions, we produced colorimetric assays that harness OR logic to activate in response to two different subtypes of HIV-1 and

AND logic to target two regions of nucleocapsid gene of SARS-CoV-2 at the same time. Application of the system to a set of positive and negative saliva samples demonstrated accurate identification of SARS-CoV-2 using a two-input multi-arm junction gate RNA.

475

476

477

478

479

480

481

482

483

484

485

486

487

488

489

490

491

492

493

494

495

496

497

498

499

500

501

502

503

504

505

506

507

Our results show that loop-initiated interactions can be very effective at driving RNA-RNA interactions in vivo and in paper-based cell-free reactions. However, effective interactions require loop domains that are sufficiently long (≥15 nt, see Supplementary Fig. 4) to provide effective binding sites and sufficient binding free energy to promote capture of the input RNA. Invasion of the input RNA into the regulator stem region further promotes the interaction and helps drive apart the remaining base pairs in the stem. In comparison to ribocomputing devices based on toehold switches, our results indicate that LIRA-based molecular logic systems generally provide lower ON/OFF ratios, likely because loop-initiated interactions are not quite as effective as toehold-initiated ones. Despite this disadvantage, we do find that LIRA-based systems offer several key benefits over toehold-switch-based circuitry¹¹. The use of multi-arm junctions for LIRA OR gate RNAs does not require translation through downstream hairpin structures and alleviates the need for long N-terminal peptides to be added to the output protein. These design features for toehold-mediated OR gates result in N-terminal peptides that increase in size by about 24 residues for each additional input detected (Supplementary Fig. 1c). This condition has led to the fusion of N-terminal peptides up to 123 residues long to the reporter protein¹¹, which corresponds to nearly half the length of GFP. Moreover, these OR gates can exhibit substantial variations in output protein expression as a function of the input RNA, yielding as much as a 14-fold difference in signal depending on the input used¹¹. For the LIRA-based OR gates reported here, the peak variation in output expression observed is 3.2-fold (Fig. 3e). Since loop-initiated OR gate performance is dominated by effects at the RNA level, as opposed to less predictable factors such as ribosome processivity and N-terminal peptide folding and translation efficiency, we expect that future refinements in LIRA OR gate secondary structure and computational design will enable higher ON/OFF ratios to be achieved.

For LIRA-based AND gates, the use of loop-initiated interactions allows sets of completely unrelated input RNA sequences to be monitored, facilitating accurate detection of two SARS-CoV-2 targets in a single paper-based colorimetric reaction. Direct detection of two pathogen targets is not possible using previously reported cell-free toehold switch assays as a result of input sequence complementarity requirements. Detection of two genomic sites simultaneously can also offer advantages compared to recently reported riboregulators with single-nucleotide specificity when targeting pathogens that are known to be mutating rapidly¹⁷.

The multi-arm junction AND gate design does require some N-terminal residues to be added to the output protein. However, the length of the additional peptide is much smaller than that used for toehold-mediated OR gate RNAs, increasing at an expected rate of about seven residues for each additional input (Supplementary Fig. 1c). Given the strengths and weaknesses of toehold-and loop-initiated interactions, we expect that future ribocomputing systems can make use of both these strategies in the same gate RNA to achieve optimal performance by maximizing dynamic range, reducing expression variability, and avoiding input sequence constraints.

CRISPR-based molecular diagnostics⁵¹⁻⁵³ have also been applied for rapid detection of SARS-CoV-2^{54,55}. These assays have demonstrated limits of detection of ~10 copies/µL in the sample⁵⁴ compared to the 60 copies/µL (or 20 aM in the amplification reaction) reported in this work for visible detection. CRISPR-based visible readout reactions have relied on lateral flow strips and targeted a single viral site in each reaction^{54,55}. Our strategy provides a simplified procedure by monitoring two SARS-CoV-2 amplicons in the same reaction. Since the paper-based riboregulator assays can be run in array formats¹⁴ and monitored directly using cameras without added light sources or filters, readout via colorimetric cell-free reactions could also enable parallel testing of larger numbers of samples than CRISPR-based assays.

We expect that the *in vivo*-validated loop-initiated motifs described here, which eliminate any correlation between the input and output sequence, will prove broadly useful for implementing a variety of other forms of RNA-based regulation, particularly those that can require strict sequence constraints, such as conditional guide RNAs⁵⁶⁻⁶⁰ and aptamer-based probes¹⁸. Moreover, the strategy for encoding molecular logic using multi-arm junction structures can also be applied to a variety of different forms of RNA output and provide the capacity to respond to multiple input species without sequence constraints. We anticipate that these capabilities will prove valuable for constructing intracellular systems that respond to endogenous RNAs to report and control cell state for biological circuits. In addition, they can be deployed in diagnostic assays to increase specificity and sensitivity, while reducing cost and test complexity to help respond to infectious disease outbreaks.

Acknowledgements

We thank Chad Simmons and Matthew Gilliam for assistance with experiments. This work was also supported by an NIH Director's New Innovator Award (1DP2GM126892), an NIH U01 award (1U01AI148319-01), an NSF RAPID award (2029532), the Gates Foundation (OPP1160667), Arizona Biomedical Research Commission funds (ADHS16-162400, CTR051763), an Alfred P.

- 541 Sloan Fellowship (FG-2017-9108), an NIH R21 award (1R21Al136571-01A1), and Canadian
- Food Inspection Agency funds (39903-200137) to A.A.G, along with funding from Salud Digna
- 543 Research Council (SDI-20166).

- **Author Contributions**
- 546 D.M. and A.A.G. conceived the RNA logic systems and wrote the manuscript. D.M., Y.X.L., and
- 547 A.A.G. designed the experiments. D.M., Y.X.L., K.Y.W., Z.Q.Y., A.A.T., S.C., and Z.M.T.
- performed the experiments. D.M. and A.A.G. analyzed the data. J.A.-F., J.L.M.-C., and A.C.-R.
- 549 collected the dengue virus serum samples.

550551

Competing Interests

- 552 D.M. and A.A.G. have filed a provisional patent application that describes aspects of this
- technology. A.A.G. is a cofounder of En Carta Inc.

554555

Data Availability Statements

- The datasets generated during and/or analysed during the current study are available from the
- 557 corresponding authors on reasonable request.

558

559

References

- 560 1. O. H. Tam, A. A. Aravin, P. Stein, A. Girard, E. P. Murchison, S. Cheloufi, E. Hodges, M.
- Anger, R. Sachidanandam, R. M. Schultz & G. J. Hannon, "Pseudogene-derived small
- interfering RNAs regulate gene expression in mouse oocytes," *Nature* **453**, 534-538
- 563 (2008).
- 564 2. E. A. Doherty & J. A. Doudna, "Ribozyme structures and mechanisms," *Annu Rev*
- 565 Biophys Biomol Struct **30**, 457-475 (2001).
- 566 3. A. Serganov & E. Nudler, "A decade of riboswitches," *Cell* **152**, 17-24 (2013).
- 567 4. J. G. Zalatan, M. E. Lee, R. Almeida, L. A. Gilbert, E. H. Whitehead, M. La Russa, J. C.
- Tsai, J. S. Weissman, J. E. Dueber, L. S. Qi & W. A. Lim, "Engineering complex synthetic
- transcriptional programs with CRISPR RNA scaffolds," *Cell* **160**, 339-350 (2015).
- 570 5. M. C. Tsai, O. Manor, Y. Wan, N. Mosammaparast, J. K. Wang, F. Lan, Y. Shi, E. Segal &
- H. Y. Chang, "Long noncoding RNA as modular scaffold of histone modification
- 572 complexes," *Science* **329**, 689-693 (2010).

- 573 6. F. J. Isaacs, D. J. Dwyer, C. Ding, D. D. Pervouchine, C. R. Cantor & J. J. Collins,
- "Engineered riboregulators enable post-transcriptional control of gene expression," Nat
- 575 Biotechnol 22, 841-847 (2004).
- 576 7. A. A. Green, P. A. Silver, J. J. Collins & P. Yin, "Toehold switches: de-novo-designed
- 577 regulators of gene expression," *Cell* **159**, 925-939 (2014).
- 578 8. A. Wittmann & B. Suess, "Engineered riboswitches: Expanding researchers' toolbox with
- 579 synthetic RNA regulators," *FEBS Letters* **586**, 2076-2083 (2012).
- 580 9. B. M. Lunde, C. Moore & G. Varani, "RNA-binding proteins: modular design for efficient
- 581 function," *Nat Rev Mol Cell Biol* **8**, 479-490 (2007).
- 582 10. L. M. Hochrein, M. Schwarzkopf, M. Shahgholi, P. Yin & N. A. Pierce, "Conditional Dicer
- substrate formation via shape and sequence transduction with small conditional RNAs," *J*
- 584 *Am Chem Soc* **135**, 17322-17330 (2013).
- 585 11. A. A. Green, J. Kim, D. Ma, P. A. Silver, J. J. Collins & P. Yin, "Complex cellular logic
- computation using ribocomputing devices," *Nature* **548**, 117-121 (2017).
- 587 12. B. Groves, Y.-J. Chen, C. Zurla, S. Pochekailov, J. L. Kirschman, P. J. Santangelo & G.
- Seelig, "Computing in mammalian cells with nucleic acid strand exchange," Nature
- 589 *Nanotechnology* **11**, 287-294 (2016).
- 590 13. G. Chatterjee, Y.-J. Chen & G. Seelig, "Nucleic Acid Strand Displacement with Synthetic
- 591 mRNA Inputs in Living Mammalian Cells," ACS Synthetic Biology 7, 2737-2741 (2018).
- 592 14. K. Pardee, A. A. Green, T. Ferrante, D. E. Cameron, A. DaleyKeyser, P. Yin & J. J. Collins,
- 593 "Paper-based synthetic gene networks," *Cell* **159**, 940-954 (2014).
- 594 15. K. Pardee, A. A. Green, M. K. Takahashi, D. Braff, G. Lambert, J. W. Lee, T. Ferrante, D.
- Ma, N. Donghia, M. Fan, N. M. Daringer, I. Bosch, D. M. Dudley, D. H. O'Connor, L.
- 596 Gehrke & J. J. Collins, "Rapid, Low-Cost Detection of Zika Virus Using Programmable
- 597 Biomolecular Components," *Cell* **165**, 1255-1266 (2016).
- 598 16. D. Ma, L. Shen, K. Wu, C. W. Diehnelt & A. A. Green, "Low-cost detection of norovirus
- 599 using paper-based cell-free systems and synbody-based viral enrichment," Synth Biol
- 600 (Oxf) **3**, ysy018 (2018).
- 601 17. F. Hong, D. Ma, K. Wu, L. A. Mina, R. C. Luiten, Y. Liu, H. Yan & A. A. Green, "Precise
- and Programmable Detection of Mutations Using Ultraspecific Riboregulators," Cell 183,

- 603 835-836 (2020).
- 604 18. S. Bhadra & A. D. Ellington, "A Spinach molecular beacon triggered by strand displacement," *RNA* **20**, 1183-1194 (2014).
- 606 19. J. K. Jung, K. K. Alam, M. S. Verosloff, D. A. Capdevila, M. Desmau, P. R. Clauer, J. W.
- Lee, P. Q. Nguyen, P. A. Pasten, S. J. Matiasek, J. F. Gaillard, D. P. Giedroc, J. J. Collins
- & J. B. Lucks, "Cell-free biosensors for rapid detection of water contaminants," Nat
- 609 Biotechnol 38, 1451-1459 (2020).
- 610 20. J. Li, A. A. Green, H. Yan & C. Fan, "Engineering nucleic acid structures for
- programmable molecular circuitry and intracellular biocomputation," Nat Chem 9,
- 612 1056-1067 (2017).
- 613 21. D. Jasinski, F. Haque, D. W. Binzel & P. Guo, "Advancement of the Emerging Field of
- 614 RNA Nanotechnology," *ACS Nano* **11**, 1142-1164 (2017).
- 615 22. Y. Weizmann & E. S. Andersen, "RNA nanotechnology-The knots and folds of RNA
- 616 nanoparticle engineering," MRS Bulletin 42, 930-935 (2017).
- 617 23. I. Severcan, C. Geary, A. Chworos, N. Voss, E. Jacovetty & L. Jaeger, "A polyhedron
- 618 made of tRNAs," *Nature Chemistry* **2**, 772-779 (2010).
- 619 24. C. Geary, P. W. K. Rothemund & E. S. Andersen, "A single-stranded architecture for
- 620 cotranscriptional folding of RNA nanostructures," *Science* **345**, 799-804 (2014).
- 621 25. D. Han, X. Qi, C. Myhrvold, B. Wang, M. Dai, S. Jiang, M. Bates, Y. Liu, B. An, F. Zhang,
- H. Yan & P. Yin, "Single-stranded DNA and RNA origami," Science 358, eaao2648
- 623 (2017).
- 624 26. M. Li, M. Zheng, S. Wu, C. Tian, D. Liu, Y. Weizmann, W. Jiang, G. Wang & C. Mao, "In
- vivo production of RNA nanostructures via programmed folding of single-stranded RNAs,"
- 626 *Nature Communications* **9**, 2196 (2018).
- 627 27. D. Liu, C. W. Geary, G. Chen, Y. Shao, M. Li, C. Mao, E. S. Andersen, J. A. Piccirilli, P. W.
- 628 K. Rothemund & Y. Weizmann, "Branched kissing loops for the construction of diverse
- 629 RNA homooligomeric nanostructures," *Nature Chemistry* (2020).
- 630 28. D. Shu, Y. Shu, F. Haque, S. Abdelmawla & P. Guo, "Thermodynamically stable RNA
- 631 three-way junction for constructing multifunctional nanoparticles for delivery of
- therapeutics," *Nature Nanotechnology* **6**, 658-667 (2011).

- Y. Nakashima, H. Abe, N. Abe, K. Aikawa & Y. Ito, "Branched RNA nanostructures for RNA interference," *Chemical Communications* **47**, 8367-8369 (2011).
- 635 30. K. A. Afonin, M. Kireeva, W. W. Grabow, M. Kashlev, L. Jaeger & B. A. Shapiro,
- "Co-transcriptional Assembly of Chemically Modified RNA Nanoparticles Functionalized
- 637 with siRNAs," *Nano Letters* **12**, 5192-5195 (2012).
- 638 31. C. J. Delebecque, A. B. Lindner, P. A. Silver & F. A. Aldaye, "Organization of Intracellular
- Reactions with Rationally Designed RNA Assemblies," *Science* **333**, 470-474 (2011).
- 640 32. G. Sachdeva, A. Garg, D. Godding, J. C. Way & P. A. Silver, "In vivo co-localization of
- enzymes on RNA scaffolds increases metabolic production in a geometrically dependent
- 642 manner," *Nucleic Acids Research* **42**, 9493-9503 (2014).
- 643 33. J. Kim, P. Yin & A. A. Green, "Ribocomputing: Cellular Logic Computation Using RNA
- 644 Devices," *Biochemistry* **57**, 883-885 (2018).
- 645 34. A. A. Green, "Synthetic bionanotechnology: synthetic biology finds a toehold in
- 646 nanotechnology," *Emerg Top Life Sci* **3**, 507-516 (2019).
- 647 35. G. Rodrigo, S. Prakash, S. Shen, E. Majer, J.-A. Daròs & A. Jaramillo, "Model-based
- design of RNA hybridization networks implemented in living cells," Nucleic Acids
- 649 Research **45**, 9797-9808 (2017).
- 650 36. J. Kim, Y. Zhou, P. D. Carlson, M. Teichmann, S. Chaudhary, F. C. Simmel, P. A. Silver, J.
- J. Collins, J. B. Lucks, P. Yin & A. A. Green, "De novo-designed translation-repressing
- riboregulators for multi-input cellular logic," Nature Chemical Biology 15, 1173-1182
- 653 (2019).
- 654 37. J. Chappell, M. K. Takahashi & J. B. Lucks, "Creating small transcription activating
- 655 RNAs," *Nat Chem Biol* **11**, 214-220 (2015).
- 656 38. A. A. Green, P. A. Silver, J. J. Collins & P. Yin, "Toehold Switches: De-Novo-Designed
- 657 Regulators of Gene Expression," *Cell* **159**, 925-939 (2014).
- 658 39. F. Hong, D. Ma, K. Wu, L. A. Mina, R. C. Luiten, Y. Liu, H. Yan & A. A. Green, "Precise
- and Programmable Detection of Mutations Using Ultraspecific Riboregulators," Cell 180,
- 660 1018-1032 (2020).
- 661 40. J. Kim, Y. Zhou, P. D. Carlson, M. Teichmann, S. Chaudhary, F. C. Simmel, P. A. Silver, J.
- J. Collins, J. B. Lucks, P. Yin & A. A. Green, "De novo-designed translation-repressing

- riboregulators for multi-input cellular logic," *Nat Chem Biol* **15**, 1173-1182 (2019).
- 41. J. N. Zadeh, C. D. Steenberg, J. S. Bois, B. R. Wolfe, M. B. Pierce, A. R. Khan, R. M.
- Dirks & N. A. Pierce, "NUPACK: Analysis and design of nucleic acid systems," *Journal of*
- 666 computational chemistry **32**, 170-173 (2011).
- 667 42. K. A. Curtis, D. L. Rudolph & S. M. Owen, "Rapid detection of HIV-1 by
- reverse-transcription, loop-mediated isothermal amplification (RT-LAMP)," J Virol
- 669 *Methods* **151**, 264-270 (2008).
- 670 43. J. Hemelaar, "The origin and diversity of the HIV-1 pandemic," Trends Mol Med 18,
- 671 182-192 (2012).
- 44. T. Gräf, H. Machado Fritsch, R. M. de Medeiros, D. Maletich Junqueira, S. Esteves de
- Matos Almeida & A. R. Pinto, "Comprehensive Characterization of HIV-1 Molecular
- Epidemiology and Demographic History in the Brazilian Region Most Heavily Affected by
- 675 AIDS," *Journal of Virology* **90**, 8160-8168 (2016).
- 676 45. T. Gräf & A. R. Pinto, "The increasing prevalence of HIV-1 subtype C in Southern Brazil
- and its dispersion through the continent," *Virology* **435**, 170-178 (2013).
- 678 46. L. Zou, F. Ruan, M. Huang, L. Liang, H. Huang, Z. Hong, J. Yu, M. Kang, Y. Song, J. Xia,
- Q. Guo, T. Song, J. He, H. L. Yen, M. Peiris & J. Wu, "SARS-CoV-2 Viral Load in Upper
- 680 Respiratory Specimens of Infected Patients," N Engl J Med 382, 1177-1179 (2020).
- 47. Z. D. Tong, A. Tang, K. F. Li, P. Li, H. L. Wang, J. P. Yi, Y. L. Zhang & J. B. Yan, "Potential
- Presymptomatic Transmission of SARS-CoV-2, Zhejiang Province, China, 2020," *Emerg*
- 683 Infect Dis **26**, 1052-1054 (2020).
- 684 48. M. M. Arons, K. M. Hatfield, S. C. Reddy, A. Kimball, A. James, J. R. Jacobs, J. Taylor, K.
- Spicer, A. C. Bardossy, L. P. Oakley, S. Tanwar, J. W. Dyal, J. Harney, Z. Chisty, J. M. Bell,
- 686 M. Methner, P. Paul, C. M. Carlson, H. P. McLaughlin, N. Thornburg, S. Tong, A. Tamin, Y.
- Tao, A. Uehara, J. Harcourt, S. Clark, C. Brostrom-Smith, L. C. Page, M. Kay, J. Lewis, P.
- Montgomery, N. D. Stone, T. A. Clark, M. A. Honein, J. S. Duchin, J. A. Jernigan, H.-S.
- Public, C. King & C. C.-I. Team, "Presymptomatic SARS-CoV-2 Infections and
- Transmission in a Skilled Nursing Facility," N Engl J Med 382, 2081-2090 (2020).
- 691 49. X. Lu, L. Wang, S. K. Sakthivel, B. Whitaker, J. Murray, S. Kamili, B. Lynch, L. Malapati, S.
- A. Burke, J. Harcourt, A. Tamin, N. J. Thornburg, J. M. Villanueva & S. Lindstrom, "US

- 693 CDC Real-Time Reverse Transcription PCR Panel for Detection of Severe Acute 694 Respiratory Syndrome Coronavirus 2," *Emerg Infect Dis* **26** (2020).
- 695 50. W. Wang, Y. Xu, R. Gao, R. Lu, K. Han, G. Wu & W. Tan, "Detection of SARS-CoV-2 in Different Types of Clinical Specimens," *JAMA* **323**, 1843-1844 (2020).
- 51. J. S. Gootenberg, O. O. Abudayyeh, M. J. Kellner, J. Joung, J. J. Collins & F. Zhang,
 "Multiplexed and portable nucleic acid detection platform with Cas13, Cas12a, and
 Csm6," *Science* **360**, 439-444 (2018).
- J. S. Chen, E. Ma, L. B. Harrington, M. D. Costa, X. Tian, J. M. Palefsky & J. A. Doudna,
 "CRISPR-Cas12a target binding unleashes indiscriminate single-stranded DNase
 activity," *Science* 360, 436-439 (2018).
- C. Myhrvold, C. A. Freije, J. S. Gootenberg, O. O. Abudayyeh, H. C. Metsky, A. F. Durbin,
 M. J. Kellner, A. L. Tan, L. M. Paul, L. A. Parham, K. F. Garcia, K. G. Barnes, B. Chak, A.
 Mondini, M. L. Nogueira, S. Isern, S. F. Michael, I. Lorenzana, N. L. Yozwiak, B. L.
 MacInnis, I. Bosch, L. Gehrke, F. Zhang & P. C. Sabeti, "Field-deployable viral diagnostics
 using CRISPR-Cas13," *Science* 360, 444-448 (2018).
- J. P. Broughton, X. Deng, G. Yu, C. L. Fasching, V. Servellita, J. Singh, X. Miao, J. A.
 Streithorst, A. Granados, A. Sotomayor-Gonzalez, K. Zorn, A. Gopez, E. Hsu, W. Gu, S.
 Miller, C.-Y. Pan, H. Guevara, D. A. Wadford, J. S. Chen & C. Y. Chiu, "CRISPR—
 Cas12-based detection of SARS-CoV-2," *Nature Biotechnology* 38, 870-874 (2020).

721

55.

M. Patchsung, K. Jantarug, A. Pattama, K. Aphicho, S. Suraritdechachai, P. Meesawat, K.

- Sappakhaw, N. Leelahakorn, T. Ruenkam, T. Wongsatit, N. Athipanyasilp, B. Eiamthong, 713 714 B. Lakkanasirorat, T. Phoodokmai, N. Niljianskul, D. Pakotiprapha, S. Chanarat, A. 715 Homchan, R. Tinikul, P. Kamutira, K. Phiwkaow, S. Soithongcharoen, 716 Kantiwiriyawanitch, V. Pongsupasa, D. Trisrivirat, J. Jaroensuk, T. Wongnate, S. Maenpuen, P. Chaiyen, S. Kamnerdnakta, J. Swangsri, S. Chuthapisith, Y. 717 718 Sirivatanauksorn, C. Chaimayo, R. Sutthent, W. Kantakamalakul, J. Joung, A. Ladha, X. 719 Jin, J. S. Gootenberg, O. O. Abudayyeh, F. Zhang, N. Horthongkham & C. Uttamapinant, 720 "Clinical validation of a Cas13-based assay for the detection of SARS-CoV-2 RNA,"
- 722 56. M. H. Hanewich-Hollatz, Z. Chen, L. M. Hochrein, J. Huang & N. A. Pierce, "Conditional

Nature Biomedical Engineering 4, 1140-1149 (2020).

- Guide RNAs: Programmable Conditional Regulation of CRISPR/Cas Function in
- 724 Bacterial and Mammalian Cells via Dynamic RNA Nanotechnology," ACS Cent Sci 5,
- 725 1241-1249 (2019).
- 726 57. K. H. Siu & W. Chen, "Riboregulated toehold-gated gRNA for programmable
- 727 CRISPR-Cas9 function," *Nat Chem Biol* **15**, 217-220 (2019).
- 728 58. L. Oesinghaus & F. C. Simmel, "Switching the activity of Cas12a using guide RNA strand
- 729 displacement circuits," *Nat Commun* **10**, 2092 (2019).
- 730 59. R. Galizi, J. N. Duncan, W. Rostain, C. M. Quinn, M. Storch, M. Kushwaha & A. Jaramillo,
- 731 "Engineered RNA-Interacting CRISPR Guide RNAs for Genetic Sensing and
- 732 Diagnostics," *CRISPR J* **3**, 398-408 (2020).
- 733 60. S. P. Collins, W. Rostain, C. Liao & C. L. Beisel, "Sequence-independent RNA sensing
- and DNA targeting by a split domain CRISPR-Cas12a gRNA switch," *Nucleic Acids Res*
- 735 (2021).

METHODS

LIRA library design

LIRAs were designed computationally using the NUPACK software package⁴¹ and selected for experimental testing using procedures reported previously⁷. Briefly, a set of 337 candidate LIRA devices were generated by NUPACK and the top 60 of these riboregulators were selected based on their ensemble defect levels. All candidate LIRAs shared the same secondary structures but differed in sequence outside of the conserved RBS, start codon, and reporter gene regions. Pairwise interactions between all the LIRAs and input RNAs were then computed to determine the expected equilibrium concentration of LIRA-input complexes formed. Using non-cognate LIRA-input complex formation probability as a crosstalk metric, a Monte Carlo selection algorithm was used to generate a library of 24 LIRAs expected to display the lowest expected overall crosstalk.

Strains and growth conditions

The following *E. coli* strains were used in this study: BL21 Star DE3 (F⁻ ompT $hsdS_B$ ($r_B^-m_B^-$) gal dcm rne131 (DE3); Invitrogen), BL21 DE3 (F⁻ ompT hsdSB ($r_B^-m_B^-$) gal dcm (DE3); Invitrogen), MG1655Pro (F⁻ λ^- ilvG- rfb-50 rph-1 Sp^R lacR tetR), and DH5 α (endA1 recA1 gyrA96 thi-1 glnV44 relA1 hsdR17($r_K^-m_{K}^+$) λ^- ; Invitrogen). All strains were grown in LB medium at 37 °C with

Plasmid construction

appropriate antibiotics.

Plasmids were constructed via PCR and Gibson assembly. Single-stranded DNAs for expressing LIRAs, gate RNAs, input RNAs were purchased from Integrated DNA Technologies and amplified into double-stranded DNA form via PCR. The amplified DNAs were then connected with plasmid backbones by 30-bp homology domains using Gibson assembly. All Gibson assembly products were transformed in the *E. coli* DH5α strain and sent out for sequence validation via Sanger sequencing. Backbones used for constructing the plasmids were amplified from the commercial vectors pET15b, pCOLADuet, and pCDFDuet (EMD Millipore) via PCR followed with DpnI treatment. The reporter protein for all plasmids is GFPmut3b with an ASV degradation tag unless otherwise noted.

Flow cytometry measurements and analysis

Bacterial colonies transformed with combinations of LIRA or gate RNA and input RNA plasmids were inoculated in 1 ml of LB in triplicate with appropriate antibiotics and grown overnight at 37° C with shaking. On the second day, 5 µl overnight-cultured medium was diluted by 100-fold in 495 µl of fresh LB with 30 µg/ml kanamycin, 50 µg/ml ampicillin and 25 µg/ml spectinomycin. After 80 min of recovery, IPTG was added into each well to a final concentration of 0.1 mM. Flow cytometry measurements were performed after 3, 4, and 5 hours of induction.

Flow cytometry was performed using a S1000 cell analyzer (Stratedigm) equipped with a high-throughput auto sampler (A600, Stratedigm). Before running measurements, cells were diluted by ~10-fold into phosphate buffered saline (PBS) in 384-well plates. Forward scatter (FSC) was used for the trigger, and ~40,000 individual cells were recorded. Cell populations were gated according to their FSC and side scatter (SSC) distributions as described previously^{7,33} (see Supplementary Fig. 9 for representative gating data). The GFP fluorescence signal outputs of these gated cells were used for following calculations. Error levels for the fluorescence measurements of ON state and OFF state cells were calculated from the SD of measurements from at least three biological replicates. The relative error levels for the ON/OFF fluorescence ratios were then determined by adding the relative errors of ON and OFF state fluorescence in quadrature.

Cell-free reactions

Cell-free transcription-translation systems (NEB, PURExpress) were prepared for freeze-drying according to following recipe: cell-free solution A, 40%; cell-free solution B, 30%; RNase Inhibitor (Roche, 03335402001, distributed by MilliporeSigma), 2%; chlorophenol red-b-D-galactopyranoside (Roche, 10884308001, distributed by MilliporeSigma, 24mg/ml), 2.5%; with the remaining volume reserved for LIRA riboregulator or gate RNA plasmids, water and lacZ α peptide added to a final concentration of 2 μ M. When testing LIRA riboregulators from a plasmid, the plasmid DNA was added to a final concentration of 30 ng/ μ l in the cell-free reaction mix. For gate RNA devices test in the paper-based system, the final concentration of the plasmid was 15 ng/ μ l.

Filter paper (Whatman, 1442-042) for depositing and freeze-drying the cell-free system was first blocked with 5% bovine serum albumin (BSA) overnight. The paper was washed three times in water for 5 to 10 min after overnight blocking. The paper was transferred on a hot plate at 50°C for drying and then cut into 2-mm diameter paper disks with a biopsy punch. The disks were then transferred into 200-µl PCR strips and 1.8 µl of the above cell-free reaction mix was

applied to each of them. Liquid nitrogen was used for freezing the PCR strips containing those paper devices. The frozen paper disks were dried overnight in a lyophilizer. Plate reader tests were carried out on the freeze-dried paper disks 2-4 days later. The systems stored in nitrogen environment, shielded from light and together with the silica gel desiccation packages as described previously¹⁴. The paper disks remained active for at least a month under storage at room temperature.

NASBA reactions

NASBA experiments were carried out using following the standard protocols: reaction buffer (Life Sciences, NECB-24; 33.5%), nucleotide mix (Life Sciences NECN-24; 16.5%), RNase inhibitor (Roche, 03335402001; 0.5%), 12.5 µM of each DNA primer (2%), nuclease-free water (2.5%) and RNA amplicon (20%) were assembled at 4°C. After being incubated at 65°C for 2 min and a 10-min incubation at 41°C, 1.25 µl of enzyme mix (Life Sciences NEC-1-24; 25%) was added to the reaction. The reaction took place at 41°C for 2 h and was then diluted 1:6 into water before applying 2 µl to the freeze-dried paper devices. For the clinical dengue samples, de-identified serum samples positive and negative for the virus were obtained at Salud Digna (Culiacan, Mexico). The sample was first diluted 10-fold into water and then heated for 2 minutes at 95°C for RNA release. The heat-extracted RNA was then added to the NASBA reaction. Heat-inactivated de-identified saliva samples positive and negative for SARS-CoV-2 were provided by the Arizona State University Biodesign Institute Clinical Testing Lab. Heat inactivation was performed by incubating samples at 65°C for 30 minutes. The saliva samples were diluted 1:1 into water and heated at 95°C for 2 minutes before spiking in NASBA reactions. A 1-µl aliquot of each sample was transferred into 5-µl NASBA reactions. Each sample was amplified using separate NASBA reactions with the corresponding primer pairs designed for each input RNA. After a 2-hour reaction, 1 µl of each pair of NASBA products was combined together and diluted with 5 µl water before adding 2 µL to the paper-based cell-free reaction.

RT-qPCR reactions

Primers were designed for both the *GFP* gene and 16S rRNA, which was used as the internal control (see Supplementary Table 11 for primer sequence information). Colonies with bacteria transformed with LIRA plasmids, toehold switch plasmids, and cognate or non-cognate input plasmids were inoculated into 6 ml LB in triplicate with appropriate antibiotics. Total RNA was extracted with a commercial RNA miniprep kit (Zymo Research, R2014) following the standard

protocol in the manual. Reverse transcription was performed using a commercial kit (Qiagen, 205311) with the protocol from the manual. PCR was performed with a commercial kit (Life Technologies, 4367659) and measured by the Mx3005P qPCR system. A no-RT control experiment was performed to confirm that no detectable DNA was present. Melting curve analysis confirmed that the qPCR product was correct.